Ore Geology Reviews 97 (2018) 143–151

Contents lists available at ScienceDirect

Ore Geology Reviews

journal homepage: www.elsevier.com/locate/oregeorev

Mass wasting events and their impact on the formation and preservation of submarine ore deposits

D.J. Smith[a,*], J. Naden[b], A.-J. Miles[b,c], H. Bennett[a], S.H. Bicknell[a]

[a] University of Leicester, University Road, Leicester LE1 7RH, UK
[b] British Geological Survey, Keyworth, Nottingham NG12 5GG, UK
[c] University of Bristol, Bristol BS8 1TH, UK

ARTICLE INFO

Keywords:
Massive sulphide
Submarine
Epithermal
Mass wasting
Seafloor

ABSTRACT

Mass wasting and landform modifying events have a profound impact on hydrothermal processes in terrestrial environments. Mass wasting events in submarine settings also modify hydrothermal systems and their associated mineralisation. We present evidence of a dynamic environment impacting on ore formation at the historically exploited Pb-Zn-(Ag) mineralisation of Triades, Milos island (Greece), formed in a submarine setting. Galena-sphalerite veins and barite-quartz gangue precipitated in the near subsurface or after exhalation of boiling hydrothermal fluids. Field evidence indicates that mineralisation was extensively reworked by debris flow events during formation. The mineral paragenetic sequence is consistent with a Pb-Zn-(Ag) massive sulphide system, and analogous to the early stages of a Kuroko-type deposit, but Triades lacks massive sulphide bodies. We suggest that mass wasting events literally truncated the developing mineral deposit as it formed on the seafloor, destroying massive sulphide bodies and limiting the development of the ore mineral assemblages. Mass wasting processes in volcanogenic massive sulphide systems are ore-destructive, with little opportunity for "telescoping", unlike terrestrial equivalents. Shallow marine systems in terrains subject to mass wasting may have low preservation potential, or may be classified as epithermal-like vein systems rather than stockwork portions of massive sulphide deposits.

1. Introduction

In the terrestrial environment it is recognised that landscape processes can significantly affect mineral deposit evolution; sector collapse at the Luise volcano had a profound impact on the formation of the giant Ladolam epithermal gold deposit (Müller et al., 2002), and progressive paleosurface degradation plays a key role in telescoping hydrothermal ore deposits (Sillitoe, 1994). However, most conceptual models of mineral deposit formation in the submarine environment envisage that mineralisation takes place in a relatively static landscape. The volcanic lithofacies of submarine and emergent volcanoes show that dome degradation, passive and explosive eruptions, and syn- and post-eruptive mass-wasting events dramatically alter the submarine landscape (Leat et al., 2010; Wright, 1996; Wright et al., 2008; Wright and Gamble, 1999), which in turn will significantly modify extant magmatic-hydrothermal and geothermal systems.

Milos island, Greece, has on-land exposures of well-preserved, young (< 3 Ma) submarine and mineralized volcanic edifices. Using sites on Milos as analogues for seafloor mineralisation (e.g. Petersen et al., 2014), here we show mass wasting events in the shallow (< 1000 m) marine environment influence deposit style and metal inventories, and negatively impact on the resource prospectivity of the seafloor.

1.1. Geological setting and submarine mineralisation of Milos

Milos is centrally located within the South Aegean Active Volcanic Arc (SAAVA) and consists of 3.5–0.1 Ma calc-alkaline volcanic domes, lavas and pyroclastic deposits built on a Mesozoic basement and upper Miocene–lower Pliocene marine sediments (Fytikas et al., 1986; Stewart and McPhie, 2006). The oldest volcanic deposits (late Pliocene) were submarine, transitioning to subaerial eruptive activity in the mid-Pleistocene (Stewart and McPhie, 2006; Stewart and McPhie, 2004). The modern, active geothermal system is considered transitional between marine and terrestrial, with contributions from magmatic volatiles, seawater, and meteoric-derived water (Naden et al., 2005).

Milos hosts a range of economic mineralisation, including marine exhalative Mn at Vani (Papavassiliou et al., 2017); epithermal Au-Ag at Profitis Ilias and Chondro Vouno (Kilias et al., 2001; Naden et al., 2005); and Zn-Pb-(Ag) deposits at Triades (Marschik et al., 2010) and

* Corresponding author.
E-mail address: djs40@le.ac.uk (D.J. Smith).

https://doi.org/10.1016/j.oregeorev.2018.05.008
Received 20 December 2017; Received in revised form 9 May 2018; Accepted 14 May 2018
Available online 16 May 2018

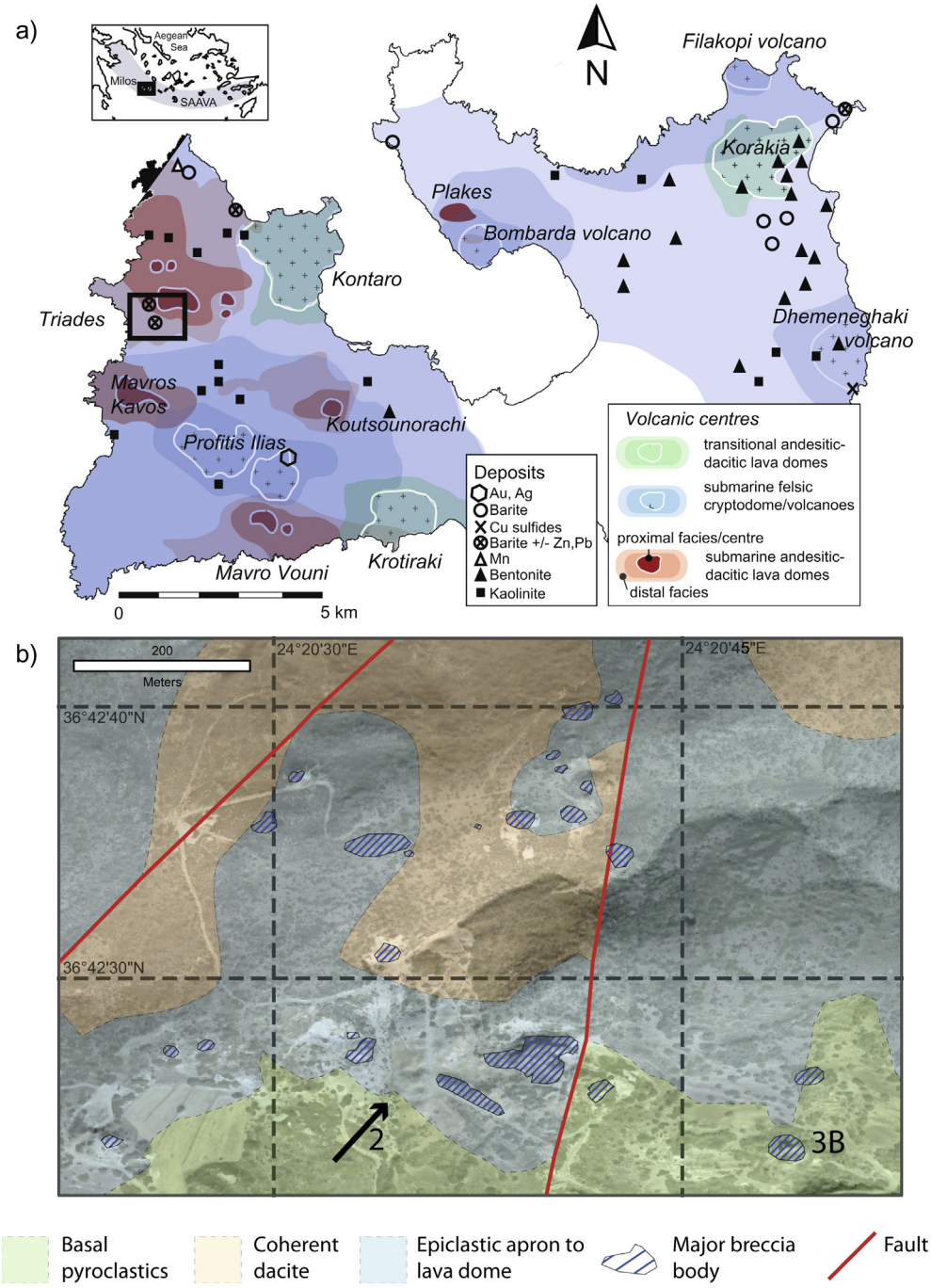

Fig. 1. (A) Simplified geological map of Milos island, showing main volcanic centres. Inset map shows position of Milos in the South Aegean Active Volcanic Arc (SAAVA). Black box shows location of map (B), a location map of the largest barite breccia domes. Arrow marks view direction for Fig. 2. Dome photographed in Fig. 3B (the main source of sulphide samples) is marked in the southeast corner of the map.

neighbouring Galana (Fig. 1). The deposits at Triades were mined from the late 19th to the early 20th century, initially for lead and zinc, and later for silver; silver reserves were estimated at 10 Mt ore at 500 ppm Ag (Liakopoulos et al., 2001). The Triades area is dominated by tuffs, hyaloclastites and debris flow deposits punctuated by partially extrusive andesitic to dacitic domes and lavas (Stewart and McPhie, 2006). Marine fossils (*Pecten* sp., *Ostrea* sp.) are contained within the volcanic sediments, confirming a relatively shallow marine environment (Marschik et al., 2010). Volcanism records emergence, determined by SHRIMP U-Pb zircon crystallisation ages from a submarine dacite at 2.18 Ma, and a subaerial equivalent at 1.44 Ma (Stewart and McPhie, 2006). Mineralisation at Triades has previously been identified as a product of a submarine hydrothermal system, classified as either Kuroko-style volcanogenic massive sulphide (VMS; Hauck, 1988; Kalogeropoulos and Mitropoulos, 1983; Vavelidis and Melfos, 1998) or intermediate to high sulphidation type epithermal mineralisation (Alfieris et al., 2013; Marschik et al., 2010).

1.2. Mass wasting deposits at Triades

In the Triades area, coherent lava domes have brecciated margins and debris aprons of hyaloclastite and reworked autobreccia (Stewart and McPhie, 2006). Intact lava domes are still present as steep-sided topographic highs (Figs. 2 and 3). The seafloor palaeotopography was

Fig. 2. View of lava domes and hydrothermal breccia domes at Triades. Solid lines show limits of coherent lava dome facies (unaltered / low grade hydrothermal alteration). Dashed lines show locations of quartz-barite breccia domes.

presumably dominated by the steep sided lava domes, much as it is now.

Mineralisation at Triades (e.g. Fig. 3C) is associated with intensely silicified (quartz) and baritized breccias, which often occur as steep sided < 10 m high domes associated with NE- and E-trending faults (Alfieris et al., 2013; Marschik et al., 2010). The barite-quartz breccia domes (Fig. 3A–B) consist of centimetre- to metre-scale, subangular to subrounded clasts of dacite, altered pumices, breccia with angular < 3 cm clasts, barite, and quartz (Fig. 3D–F). All the clasts show alteration to adularia-sericite, or are partially to wholly baritized and silicified. Clasts are cemented by a barite-quartz mix, and in some cases are supported or enveloped in a massive or crystalline matrix of barite and

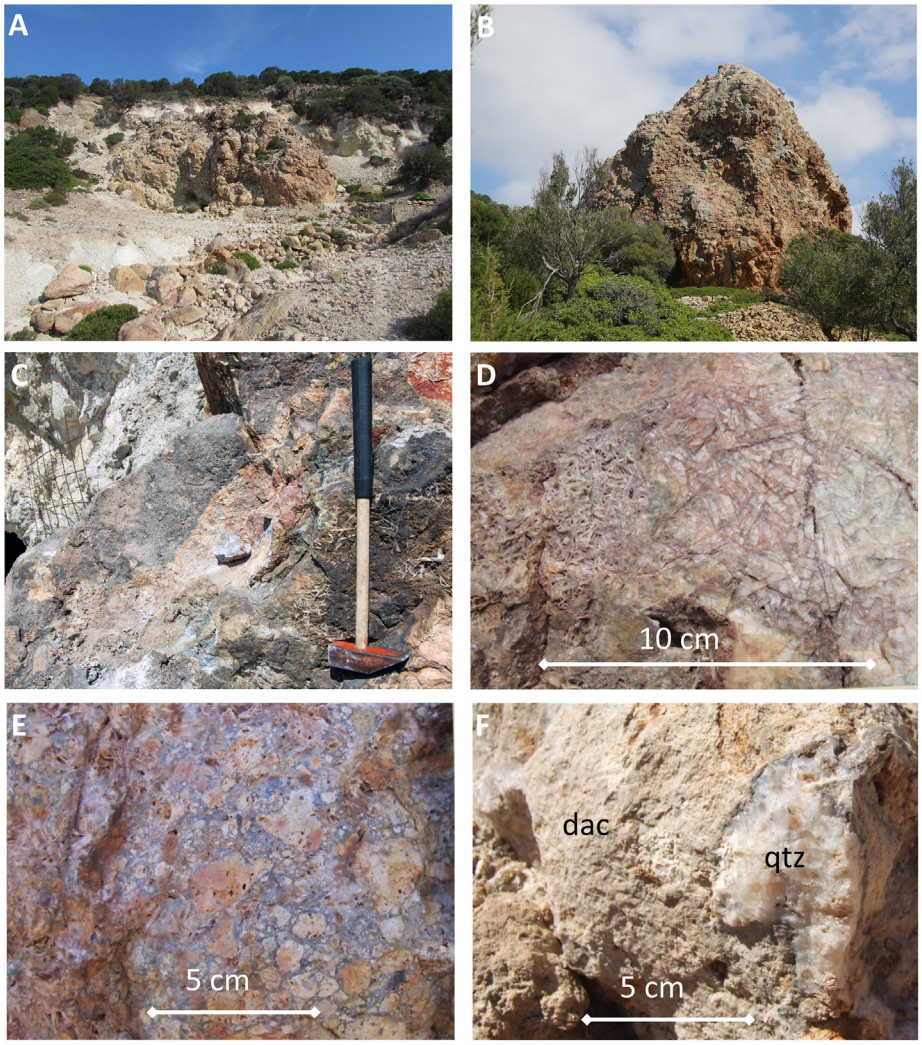

Fig. 3. Typical lithologies at the Triades area, Milos. A) Barite-quartz breccia mounds host pods of sulphide mineralisation, typically at the base (note small pit/ adit). Height of face approx. 3 m. Sulphide samples for this study were dominated by samples from an *in situ* pod at the base of a large mound (B). Within the breccia mounds are: C) sulphide pod(s), this one from the mound in 3B; D) cobbles of ~ 100% barite laths; E) clasts of silicified and baritized phreato-magmatic breccias; F) hydrothermally altered volcanic rock (dac = dacite) and hydrothermal minerals (qtz = quartz; barite also occurs). The clasts are typically cemented in quartz and/or barite, and many show quartz and barite clasts in quartz and barite cement.

quartz (e.g. Fig. 3D). Multiple generations of quartz and/or barite-filled veins cut individual clasts, as well as the domes. Late stage crystalline quartz and barite envelopes the dome surfaces and dilated fractures, and often exhibits euhedral, void filling textures. Sulphide ore minerals are found in the matrix of the barite-quartz breccias, or as pod-like veins and lenses (< 1 m^3 in volume) at the base of the breccia domes, although a long history of mining means relatively little *in situ* mineralisation remains.

Clasts of reworked barite (with and without sulphide ore) in barite-cemented breccias are evidence of periodic or continual reworking of the partially exhalative hydrothermal mineralisation, and variably altered volcaniclastic material in the breccias suggest input from lava domes. The geological evidence points towards the repeated growth of over-steepened domes comprising both lava and hydrothermal minerals, with partial and complete collapses and re-cementation of the brecciated material.

2. Results

Barite (± silica) samples were collected from various breccia mounds in the Triades area (Fig. 1B), with particular emphasis on the highlighted mound (Fig. 3B). This latter mound has exposed, *in situ* pods of sulphides at its base (Fig. 3C); the sulphide samples described below were sourced from this mound. Sulphides bodies in other mounds have either been worked out by miners, or are distributed as occurrences within barite clasts. Samples were analysed through optical microscopy (samples prepared into nine polished thin sections, and thirteen polished blocks for reflected light analysis), supplemented by major element microanalysis from the British Geological Survey's FEI QUANTA 600 environmental scanning electron microscope, equipped with an Oxford Instruments INCA Energy 450 energy-dispersive X-ray microanalysis (EDXA) system, with an Oxford Instruments X-Max large area (50 mm^2) Peltier-cooled silicon-drift detector (SSD).

2.1. Mineral paragenesis

The sulphide assemblage includes galena and sphalerite, with less abundant pyrite, chalcopyrite, and tennantite–tetrahedrite. Previous authors have also observed enargite (Alfieris et al., 2013). A series of samples from an *in situ*, sulphide-bearing vein system have been organised into a series of stages (Fig. 4). Stage 1 is euhedral barite laths, which reach up to 3 cm on the longest axis (Fig. 5A and B). Clasts of massive barite with laths up to 10 cm are also found in the mounds that host the veins. Stage 1 barite laths in veins are overgrown by Stage 2 minerals (Figs. 5A–C and 6) – an assemblage dominated by coarse (up to 0.5 cm wide) subhedral quartz crystals (up to 60% by volume), barite, variable amounts of sulphide minerals (< 2 mm sphalerite crystals with rare inclusions of chalcopyrite and pyrite; Figs. 5C and 6B) and chalcedony with late, fine (50–500 μm) subhedral quartz (Fig. 5D). In sulphide-rich portions, the chalcedony and quartz are poorly developed or absent.

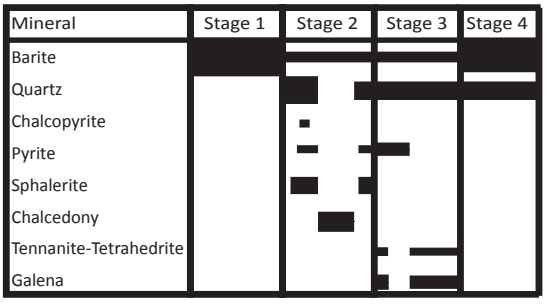

Fig. 4. Simplified paragenetic sequence of sulphide and major gangue minerals at Triades.

Stages 1 and 2 are cut or partially replaced by Stage 3 veins, composed of fine grained (50–500 μm) subhedral quartz with interspersed 10 μm barite laths. In galena-poor veins, they are accompanied by colloform-banded pyrite (Fig. 6C) and rare sphalerite. Rare tetrahedrite and tennantite bands occur within the pyrite. Rare copper sulphides (covellite, bornite and chalcopyrite) occur, likely of supergene origin (Fig. 6D). Galena commonly has a graphic texture, intergrown with quartz with crystals up to 3 mm in length (Fig. 6E and F). Galena often veins and replaces sphalerite, and often contains inclusions of tennantite-tetrahedrite (Fig. 6B).

Stage 4 is composed of large, euhedral quartz and barite crystals, up to 3 cm on the longest axis, and show void-filling textures – indeed, can be seen partially filling extant voids and open fractures. No sulphide mineralisation is associated with this stage, and it crosscuts earlier stages (Fig. 5E).

2.2. Fluid inclusion microthermometry

Six quartz, barite, and translucent sphalerite-bearing samples were prepared as doubly polished 100–200 μm thick wafers for fluid inclusion microthermometry. The samples were investigated with a transmitted light petrographic microscope to identify primary inclusions free of deformation, leakage or decrepitation; these were liberated from the wafer by microcoring a subsection, and immersing in methanol at room temperature to remove any mounting adhesive. Microthermometric studies were carried out using Linkam MDS-600 heating-freezing stages at the University of Leicester and the British Geological Survey, Keyworth. The stages were calibrated with commercially available H_2O and H_2O-CO_2 synthetic fluid inclusion standards.

Fluid inclusions in barite are susceptible to stretching, and as such may produce unreliable data – in particular, an overestimate of trapping temperature (Bodnar and Bethke, 1984; Rife, 1971). The impact of stretching on barite inclusions was minimized by selecting only regularly-shaped primary inclusions, by heating before freezing (to reduce mechanical impacts of ice formation), and by measurement of inclusion and vapour bubble areas before and after heating and freezing. Any inclusions that showed a permanent change in size, or a permanent size change in contained vapour bubbles, are considered to have stretched or leaked and have been rejected from the dataset. T_h achieved during previous microthermometric studies of barites from Triades (260–340 °C, Vavelidis and Melfos, 1998; 290–305 °C Ballanti, 1997) are at least 30 °C greater than the highest temperatures measured in this study. Deformation on heating of these authors' inclusions may have occurred, yielding higher reported temperatures. Salinity estimates were determined from $T_{m\text{-}ice}$, assuming NaCl as the only contributor of salinity, using Steele-MacInnis et al. (2011).

In total, microthermometric data were obtained from 94 fluid inclusions hosted in early barite (Stage 1), matrix barite (Stage 2), barren quartz (Stage 2), ore-associated quartz (Stage 2 and 3), sphalerite (Stage 2) and euhedral, cross-cutting barite and quartz (Stage 4). Chalcedonic silica did not contain measurable fluid inclusions. Microthermometric data are presented in Fig. 7.

First ice melting temperatures ($T_{fm\text{-}ice}$) of inclusions, where observed, occur between −30 °C and −21 °C, and suggest that the fluids in terms of their cations, are NaCl dominated, though temperatures in the region of −30 °C indicate the possible presence of divalent cations such as magnesium. Final ice melting temperatures ($T_{m\text{-}ice}$) range −0.2 to −5.2 °C (median: −3.1 °C), which correspond to salinities between 0.35 and 8.14 wt% NaCl eq. (Median: 5.1 wt% NaCl eq.). Homogenisation temperatures (T_h) vary from 110 to 372 °C (Median: 202 °C). High temperatures (> 320 °C) are exclusively recorded in barite and probably represent necked/leaked inclusions. Excluding these data (n = 2) all other inclusions homogenise below 250 °C. Fig. 7 shows the frequency distributions of T_h, salinity and how they co-vary with data discriminated by hosting mineral phase. From this a number of observations can be made:

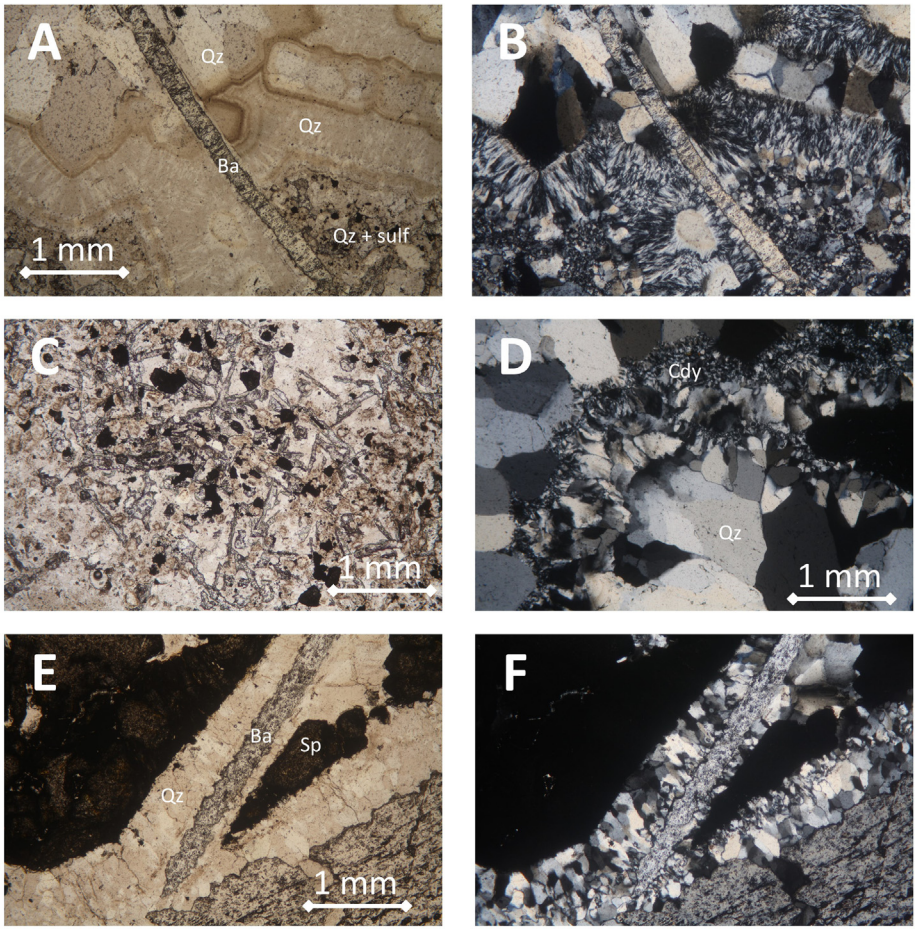

Fig. 5. Transmitted light photomicrographs of breccia mound material. A and B) Stage 1 euhedral barite laths enclosed in Stage 2 quartz (larger crystals) and later finely crystalline quartz and Stage 2 sulphides; in plane polarised and cross polarised light. C) Stage 2 quartz, barite and sulphides (opaque / black). Sample is representative of typical occurrence of sulphides within breccia mounds, outside of more massive sulphide pods (c.f. Fig. 3B). D) Chalcedony and quartz (Stage 2). E and F) Stage 2 sphalerite crosscut by barren veins of quartz and barite (Stage 4). Abbreviations: Qz quartz; Ba barite; Cdy chalcedony; Sp sphalerite.

1. Most of the data fall in vertical to sub-vertical arrays where rapidly increasing salinity (c. 3–8 wt% NaCl equiv) is associated with a gradual decrease in homogenisation temperature (220–180 °C). This trend is analogous to that recorded in the nearby Profitis Ilias Au-Ag deposit where it is interpreted to be the result of extensive open system boiling (Kilias et al., 2001, Naden et al., 2005), where the highest homogenisation temperatures and lowest salinities represent the composition of the hydrothermal fluid at initial boiling with the higher salinity, lower T_h inclusions characterising the boiled residual fluid.
2. Though most of the data exhibit salinities in excess of seawater, a group of 15 inclusions hosted in fault-hosted quartz and sphalerite have salinities of 1.5 wt% NaCl eq, or less. This somewhat mirrors the low salinity–high T_h inclusions recorded at Profitis Ilias (Kilias et al. 2001). However, at Triades anomalously high T_h inclusions (Th > 300 °C) are absent. At Profitis Ilias, this type of T_h-Salinity trend was interpreted to result from the trapping of condensed vapour with or without co-existing brine.
3. Primary fluid inclusions hosted in sphalerite provide direct evidence for the composition and temperature of the mineralizing fluid, hosting both low-salinity (wt% NaCl eqiv. < 1.5) and higher salinity inclusions (wt% NaCl equiv: ~4.5–8.5). Quartz associated with ore has similar composition (wt% NaCl equiv: ~3–7) and T_h (200–210 °C) as the higher salinity sphalerites (T_h: 180–210 °C). For barite-hosted fluid inclusions, there is no sub seawater salinity population, but in the higher salinity population salinities are similar to quartz and sphalerite. T_h shows significantly more scatter (~110–380 °C), which is probably due in part to post-trapping modifications. Nonetheless, T_h in the majority of barite-hosted fluid inclusions is consistent with that recorded in other minerals (~180–220 °C), with some evidence for lower temperatures (~110–180 °C), which may reflect mixing with cooler seawater.

2.3. Pressure–temperature considerations

Comparing the distribution of T_h–salinity data at Triades with the nearby Profitis Ilias and Chondro Vouno Au-Ag deposits (Kilias et al. 2001; Naden et al. 2005) it is reasonable to conclude, by analogy, that the processes of open system boiling also operated at Triades, albeit at lower temperatures. Thus, as boiling was an integral part of the mineralisation process, fluid inclusion T_h is the trapping temperature of the hydrothermal fluid and consequently the vapour pressure at homogenisation is the trapping pressure. Taking fluid inclusions with salinities of 3.5 wt% NaCl equiv. that homogenise at 210 °C to be representative of the hydrothermal fluid at initial boiling (see 1. above), we can estimate fluid densities and vapour pressures of 0.88 gcm^{-3} and 1.58 MPa (calculated using Bakker, 2003). This corresponds to a hydrostatic head of 183 m. This indicates that the maximum water depth during the partially exhalative mineralisation at Triades was around 200 m.

3. Discussion

The Triades deposit is hosted by, and syngenetic with, sedimentary lithofacies formed by mass-wasting events in a shallow submarine environment. Reworked hydrothermal minerals in the mineralized breccia domes demonstrate that shallow seafloor and exhalative processes were accompanied by continual or intermittent dome failure and debris-reworking. The incorporation of variably-altered volcanic material alongside sulphide, barite and quartz clasts indicates that material

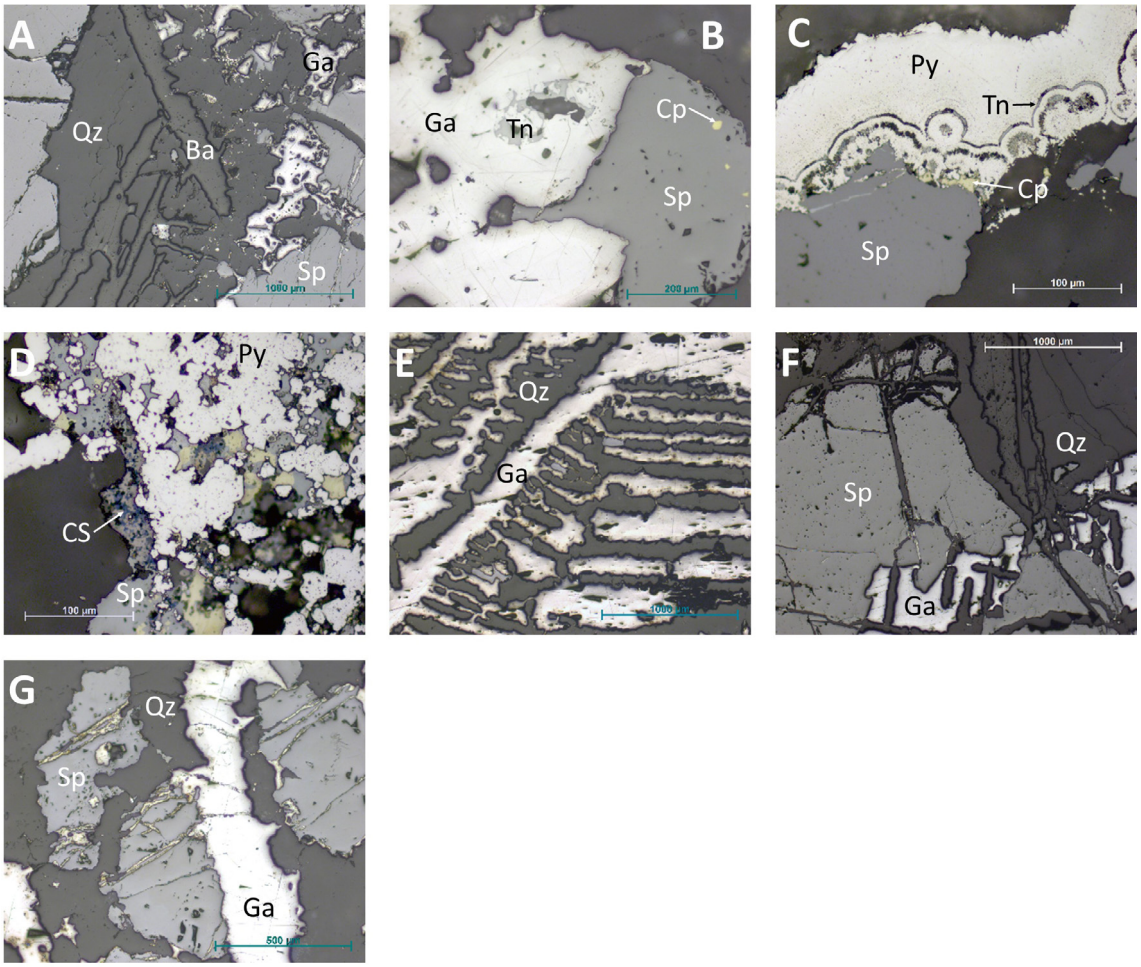

Fig. 6. Reflected light photomicrographs of polished blocks of mineralized material. A) Euhedral barite laths with quartz and sphalerite; galena veining and replacing sphalerite. B) Galena and sphalerite. Sphalerite contains inclusions of chalcopyrite; galena contains inclusions of tennantite and tetrahedrite. C) Colloform pyrite on sphalerite. Pyrite includes bands of tennantite, tetrahedrite and chalcopyrite. D) Sphalerite and pyrite with possibly supergene copper sulphides (bornite and covellite). E) Graphic intergrowth of galena and quartz. F) Galena veining and replacing sphalerite. Late quartz laths along galena cleavage and veining sphalerite. G) Galena veining and replacing sphalerite in quartz matrix. Abbreviations: Ba barite; Qz quartz; Sp sphalerite; Ga galena, Tn tennantite-tetrahedrite; Cp chalcopyrite; Py pyrite; CS copper sulphides.

derived from relatively unaltered lava domes also contributed to the clastic inputs into the deposit.

The mineral paragenesis is consistent with precipitation from fluids with temperatures that decline from the onset of sulphide precipitation. The decreasing temperature of the systems is reflected in the increasing galena:sphalerite ratio (Reed and Palandri, 2006) and the replacement of Stage 2 and 3 pyrite with Stage 3 tennantite (Knight, 1977). Stage 2 sphalerite is interrupted or absent where chalcedony occurs, consistent with an ephemeral departure to lower fluid temperatures (such that amorphous silica is favoured over quartz precipitation). We interpret the evolution of the Triades mineral assemblage as a product of hydrothermal fluids boiling in an open system (~210 °C) precipitating Stage 1 gangue and Stage 2 sulphides, interrupted by lower temperature (< 200 °C) intervals. This is followed by a progressive decline in temperature to Stage 3 (< 180 °C).

Combining the evidence for mass wasting with the mineral paragenesis, we interpret Triades to be formed from a venting hydrothermal system (Fig. 8). Triades lacks exhalative massive sulphide lenses; in an environment subject to mass wasting events, they would be disrupted and destroyed. Barite-cemented breccia “mounds” formed around discharge points, likely a result of the rapid precipitation of barite at the hydrothermal – seawater interface. The inability of the system to maintain a carapace of sulphides and sulphates led to marine incursions that lowered the temperature of the final mixed fluid, diluted ore forming minerals, and precipitated barite in veins.

Hydrothermal barite deposition and reworking are associated with massive sulphide mineralisation of Wetar Island, Indonesia (Scotney et al., 2005). Triades shows significantly less sulphide mineralisation than the Wetar Island deposits, where barite capped the sulphide orebodies, and sedimentation (limestone, gypsum and chert) further protected the sulphide lenses from destruction (Scotney et al., 2005). The lower abundance of sulphides at Triades may reflect a combination of a mass-wasting, erosive environment, and a shorter-lived hydrothermal system.

The final mineral assemblage at Triades is analogous to the waxing (pre-ore and “black ore”) stages of a Kuroko-type massive sulphide deposit (Ohmoto, 1996) – a deposit class in which Triades has previously been placed (Vavelidis and Melfos, 1998). However, compared to a typical Kuroko-type deposit, Triades lacks massive sulphide bodies and later Cu-sulphide and pyrite-rich ore stages. Whilst the absence of massive sulphide bodies is consistent with mass wasting, the absence of the pyritic and Cu-rich ore zones at Triades can be attributed to the shallow depth of formation at Triades. Fluid inclusion data demonstrate that hydrothermal fluids were at a low enough pressure to be in the two phase (boiling) field, and Milos had been below < 1000 m water depth for ~5 My (Van Hinsbergen et al., 2004). At water depths less than < 1000 m, Cu sulphides are rarely precipitated in abundance (Monecke et al., 2014); fluids cannot be discharged at a high enough

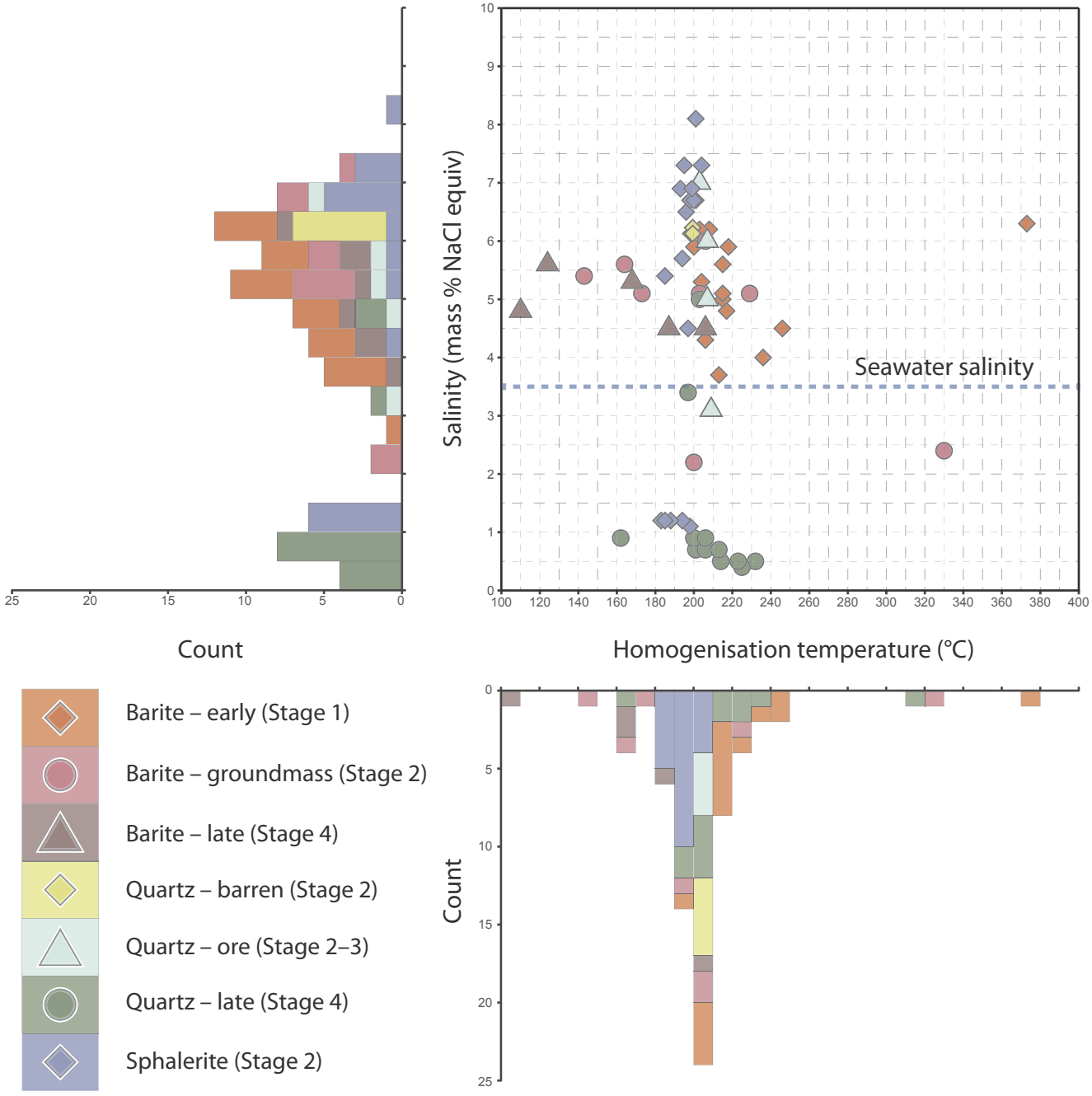

Fig. 7. Scattergram of homogenisation temperature versus salinity with marginal histograms with individual points and histogram ranges discriminated by host mineral and paragenetic stage (see text for detail).

temperature (> 300 °C) to transport significant Cu (Ohmoto, 1996) due to boiling.

Triades has been previously described as an epithermal-type deposit (Alfieris et al., 2013; Marschik et al., 2010) because of the vein-hosted style of the present day deposit. Unlike on-shore epithermal systems, submarine vein systems have no capacity to "telescope" (Sillitoe, 1994) during mass wasting events. In on-shore systems, mass wasting removes hydrostatic load, and the pressure drop triggers boiling of the hydrothermal system, and/or overprints boiling zones over deeper parts of the system. Boiling is a key ore-forming mechanism, and the overprinting or telescoping of boiling zones can enhance ore grade (Sillitoe, 1994). In the submarine environment, hydrostatic load is controlled by sea level, and the loss of a column of rock has a minimal effect on the hydrostatic pressure. The boiling zone of submarine systems remains fixed at a particular depth relative to sea level, with no role for moving the boiling zone in the rock column to achieve telescoping. Thus, mass wasting has no positive impact on ore precipitation and grade in the vein/stockwork portions of submarine systems, and is destructive of the exhalative portions.

Following mass wasting events, sulphides may be re-deposited in clastic, stratiform horizons that contribute to ore reserves (e.g. Eskay Creek; Sherlock et al., 1999), but this is highly dependent on depositional regime. Mass wasting is a near-ubiquitous process yet has no positive effect on either ore grade or tonnage for deposits. Modern seafloor deposits are only capturing a fraction of the metal flux carried by hydrothermal fluids, and not all vents are accompanied by sulphide accumulations (Hannington et al., 2011). Mass wasting will be a contributing factor to uneconomic hydrothermal vents.

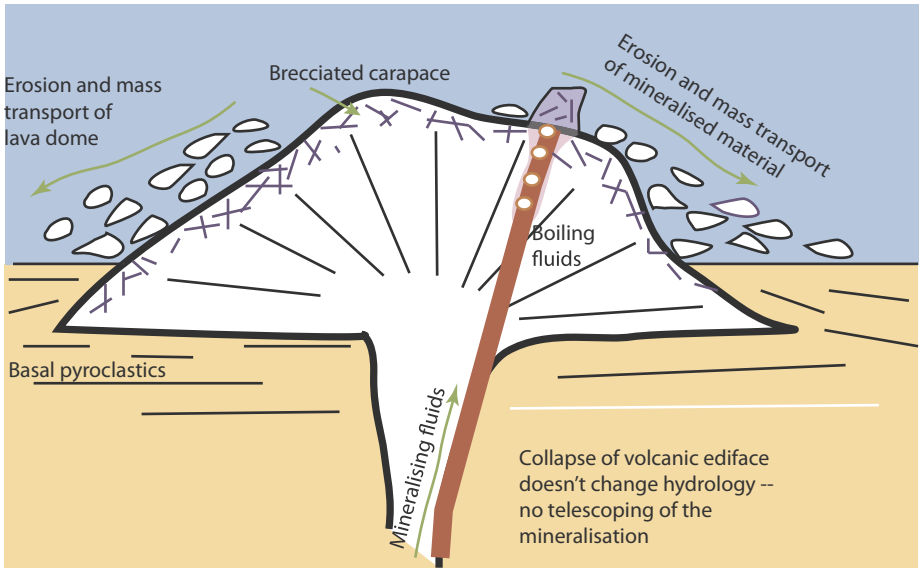

Fig. 8. Conceptual model of mineralisation at Triades. Fluids circulate through basal pyroclastics and lava domes (or cryptodomes), and boil in the subsurface. Mass wasting events transport clasts of dome material, and rework exhalative portions of hydrothermal deposits. Sulphide mineralisation is reworked, or left intact in stockwork portions only.

In submarine settings, truncated deposits would not be viable mineral resources, given the technical challenges of mining vein-hosted ore underwater. Prospectivity and resource assessments for submarine massive sulphides have emphasised tectonic setting and host rock composition (e.g. German et al., 2016) but topographic controls on mass wasting and deposition will play a role in deposit size. Environments with net deposition of sediments, or capping lava flows (Herrington et al., 2005), are more likely to preserve large deposits (c.f. mineralisation at Wetar; Scotney et al. 2005) than those with net denudation, but conversely be harder to discover in marine settings due to burial. Marine analogues are those exposed at the seafloor, and this perhaps is the reason why onshore VMS deposits are much larger than submarine equivalents discovered to date (Hannington et al., 2010).

4. Conclusions

Mineralisation at Triades has been limited by mass-wasting events in the shallow submarine environment. Over-steepened domes and subsequent collapse truncated the developing mineral deposit and destroyed any massive sulphide bodies that were forming. Poor preservation potential within this dynamic environment resulted in an unviable mineral resource despite net deposition of sediment. Boiling is the main ore-forming mechanism with topography being the major control on mineralisation.

The mineral assemblage exhibited can be divided into multiple stages, with open system boiling hydrothermal fluids reaching at approximately 210 °C in early stages, followed by lower temperature (< 200 °C) intervals and a final progressive decline (< 180 °C). Metal mineralisation is limited to a 210–150 °C window, which was likely interrupted by mass-wasting.

Acknowledgments

This work was supported by the Natural Environment Research Council (UK) grants NE/M010848/1, NE/N019040/1, the NERC GW4 + Doctoral Training Partnership, and the British Geological Survey's University Funding Initiative (BUFI). A-JPM is supported by a NERC DTP studentship (NE/L002434/1) and the BGS University funding initiative (BUFI S345). JN publishes with the permission of the Executive Director, The British Geological Survey (NERC).

Appendix A. Supplementary data

Supplementary data associated with this article can be found, in the online version, at http://dx.doi.org/10.1016/j.oregeorev.2018.05.008.

References

Alfieris, D., Voudouris, P., Spry, P.G., 2013. Shallow submarine epithermal Pb-Zn-Cu-Au-Ag-Te mineralisation on western Milos Island, Aegean Volcanic Arc, Greece: mineralogical, geological and geochemical constraints. Ore Geol. Rev. 53, 159–180.
Bakker, R.J., 2003. Package FLUIDS 1. Computer programs for analysis of fluid inclusion data and for modelling bulk fluid properties. Chem. Geol. 194 (1), 3–23.
Ballanti, D.D., 1997. Origin of the bentonite and barite deposits on Milos Island (Central Aegean, Greece). Swiss Federal Institute of Technology. pp. 237.
Bodnar, R.J., Bethke, P.M., 1984. Systematics of stretching of fluid inclusions; I, Fluorite and sphalerite at 1 atmosphere confining pressure. Econ. Geol. 79 (1), 141–161.
Fytikas, M., et al., 1986. Volcanology and petrology of volcanic products from the island of Milos and neighbouring islets. J. Volcanol. Geotherm. Res. 28 (3–4), 297–317.
German, C.R., Petersen, S., Hannington, M.D., 2016. Hydrothermal exploration of mid-ocean ridges: where might the largest sulfide deposits be forming? Chem. Geol. 420, 114–126.
Hannington, M., Jamieson, J., Monecke, T., Petersen, S., 2010. Modern sea-floor massive sulfides and base metal resources: toward an estimate of global sea-floor massive sulfide potential. Soc. Econ. Geol. Spec. Public. 15, 317–338.
Hannington, M., Jamieson, J., Monecke, T., Petersen, S., Beaulieu, S., 2011. The abundance of seafloor massive sulfide deposits. Geology 39 (12), 1155–1158.
Hauck, M., 1988. Kuroko-type ore deposits on the Aegean Islands, Greece, Base Metal Sulfide Deposits in Sedimentary and Volcanic Environments. Springer 216–228.
Herrington, R.J., Zaykov, V.V., Maslennikov, V.V., Brown, D., Puchkov, V.N., 2005. Mineral deposits of the Urals and links to geodynamic evolution. Econ. Geol. 100 (S), 1069–1095.
Kalogeropoulos, S., Mitropoulos, P., 1983. Geochemistry of barites from Milos Island (Aegean Sea), Greece. Neues Jahrbuch Fur Mineralogie-Monatshefte 1, 13–21.
Kilias, S.P., et al., 2001. Epithermal gold mineralisation in the active Aegean Volcanic Arc: the Profitis Ilias deposit, Milos Island, Greece. Mineral. Depos. 36, 32–44.
Knight, J.E., 1977. A thermochemical study of alunite, enargite, luzonite, and tennantite deposits. Econ. Geol. 72 (7), 1321–1336.
Leat, P.T., Tate, A.J., Tappin, D.R., Day, S.J., Owen, M.J., 2010. Growth and mass wasting of volcanic centers in the northern South Sandwich arc, South Atlantic, revealed by new multibeam mapping. Mar. Geol. 275 (1–4), 110–126.
Liakopoulos, A., Glasby, G.P., Papavassiliou, C.T., Boulegue, J., 2001. Nature and origin of the Vani manganese deposit, Milos, Greece: an overview. Ore Geol. Rev. 18 (3–4), 181–209.
Marschik, R., Bauer, T., Hensler, A.-S., Skarpelis, N., Hölzl, S., 2010. Isotope Geochemistry of the Pb-Zn-Ba(-Ag-Au) mineralization at Triades-Galana, Milos Island, Greece. Resour. Geol. 60 (4), 335–347.
Monecke, T., Petersen, S., Hannington, M.D., 2014. Constraints on water depth of massive sulfide formation: evidence from modern seafloor hydrothermal systems in arc-related settings. Econ. Geol. 109 (8), 2079–2101.
Müller, D., et al., 2002. The transition from porphyry- to epithermal-style gold mineralization at Ladolam, Lihir Island, Papua New Guinea: a reconnaissance study. Mineral. Depos. 37 (1), 61–74.
Naden, J., Kilias, S.P., Darbyshire, D.P.F., 2005. Active geothermal systems with entrained seawater as modern analogues for transitional volcanic-hosted massive sulfide and continental magmato-hydrothermal mineralization: the example of Milos

Island, Greece. Geology 33 (7), 541–544.
Ohmoto, H., 1996. Formation of volcanogenic massive sulfide deposits: The Kuroko perspective. Ore Geol. Rev. 10 (3–6), 135–177.
Papavassiliou, K., et al., 2017. New geochemical and mineralogical constraints on the genesis of the Vani hydrothermal manganese deposit at NW Milos island, Greece: Comparison with the Aspro Gialoudi deposit and implications for the formation of the Milos manganese mineralization. Ore Geol. Rev. 80, 594–611.
Petersen, S., et al., 2014. Drilling shallow-water massive sulfides at the Palinuro volcanic complex, Aeolian island arc, Italy. Econ. Geol. 109 (8), 2129–2158.
Reed, M.H., Palandri, J., 2006. Sulfide mineral precipitation from hydrothermal fluids. Rev. Mineral. Geochem. 61 (1), 609–631.
Rife, D.L., 1971. Barite fluid inclusion geothermometry, Cartersville mining district, northwest Georgia. Econ. Geol. 66 (8), 1164–1167.
Scotney, P.M., Roberts, S., Herrington, R.J., Boyce, A.J., Burgess, R., 2005. The development of volcanic hosted massive sulfide and barite–gold orebodies on Wetar Island, Indonesia. Miner. Depos. 40 (1), 76–99.
Sherlock, R.L., Roth, T., Spooner, E.T.C., Bray, C.J., 1999. Origin of the Eskay Creek precious metal-rich volcanogenic massive sulfide deposit; fluid inclusion and stable isotope evidence. Econ. Geol. 94 (6), 803–824.
Sillitoe, R.H., 1994. Erosion and collapse of volcanoes; causes of telescoping in intrusion-centered ore deposits. Geology 22 (10), 945–948.
Steele-MacInnis, M., Bodnar, R.J., Naden, J., 2011. Numerical model to determine the composition of H_2O–NaCl–$CaCl_2$ fluid inclusions based on microthermometric and microanalytical data. Geochim. Cosmochim. Acta 75 (1), 21–40.
Stewart, A., McPhie, J., 2006. Facies architecture and Late Pliocene – Pleistocene evolution of a felsic volcanic island, Milos, Greece. Bull. Volcanol. 68 (7), 703–726.
Stewart, A.L., McPhie, J., 2004. An Upper Pliocene coarse pumice breccia generated by a shallow submarine explosive eruption, Milos, Greece. Bull. Volcanol. 66 (1), 15–28.
Van Hinsbergen, D., et al., 2004. Vertical motions in the Aegean volcanic arc: evidence for rapid subsidence preceding volcanic activity on Milos and Aegina. Mar. Geol. 209 (1), 329–345.
Vavelidis, M., Melfos, V., 1998. Fluid inclusion evidence for the origin of the barite silver-gold-bearing Pb-Zn mineralization of the Triades area, Milos island, Greece. Bull. Geol. Soc.Greece XXXII/3, 137–144.
Wright, I.C., 1996. Volcaniclastic processes on modern submarine arc stratovolcanoes: sidescan and photographic evidence from the Rumble IV and V volcanoes, southern Kermadec Arc (SW Pacific). Mar. Geol. 136 (1–2), 21–39.
Wright, I.C., et al., 2008. Collapse and reconstruction of Monowai submarine volcano, Kermadec arc, 1998–2004. J. Geophys. Res. Solid Earth 113 (B8), B08S03.
Wright, I.C., Gamble, J.A., 1999. Southern Kermadec submarine caldera arc volcanoes (SW Pacific): caldera formation by effusive and pyroclastic eruption. Mar. Geol. 161 (2–4), 207–227.